



Article

Effect of Bacterial Amyloid Protein Phenol–Soluble Modulins Alpha 3 on the Aggregation of Amyloid Beta Protein Associated with Alzheimer’s Disease

Bushu Peng , Shaoying Xu , Yue Liang, Xiaoyan Dong * and Yan Sun *

Department of Biochemical Engineering, School of Chemical Engineering and Technology, Key Laboratory of Systems Bioengineering and Frontiers Science Center for Synthetic Biology (Ministry of Education), Tianjin University, Tianjin 300350, China; shuzi0410@tju.edu.cn (B.P.); tinaxu@tju.edu.cn (S.X.); liangyue@tju.edu.cn (Y.L.)

* Correspondence: d_xy@tju.edu.cn (X.D.); ysun@tju.edu.cn (Y.S.); Tel.: +86-22-27403389 (Y.S.)

Abstract: Since the proposal of the brainstem axis theory, increasing research attention has been paid to the interactions between bacterial amyloids produced by intestinal flora and the amyloid β -protein ($A\beta$) related to Alzheimer’s disease (AD), and it has been considered as the possible cause of AD. Therefore, phenol–soluble modulins (PSM) $\alpha 3$, the most virulent protein secreted by *Staphylococcus aureus*, has attracted much attention. In this work, the effect of PSM $\alpha 3$ with a unique cross– α fibril architecture on the aggregation of pathogenic $A\beta_{40}$ of AD was studied by extensive biophysical characterizations. The results proposed that the PSM $\alpha 3$ monomer inhibited the aggregation of $A\beta_{40}$ in a concentration–dependent manner and changed the aggregation pathway to form granular aggregates. However, PSM $\alpha 3$ oligomers promoted the generation of the β -sheet structure, thus shortening the lag phase of $A\beta_{40}$ aggregation. Moreover, the higher the cross– α content of PSM $\alpha 3$, the stronger the effect of the promotion, indicating that the cross– α structure of PSM $\alpha 3$ plays a crucial role in the aggregation of $A\beta_{40}$. Further molecular dynamics (MD) simulations have shown that the Met1–Gly20 region in the PSM $\alpha 3$ monomer can be combined with the Asp1–Ala2 and His13–Val36 regions in the $A\beta_{40}$ monomer by hydrophobic and electrostatic interactions, which prevents the conformational conversion of $A\beta_{40}$ from the α -helix to β -sheet structure. By contrast, PSM $\alpha 3$ oligomers mainly combined with the central hydrophobic core (CHC) and the C-terminal region of the $A\beta_{40}$ monomer by weak H-bonding and hydrophobic interactions, which could not inhibit the transition to the β -sheet structure in the aggregation pathway. Thus, the research has unraveled molecular interactions between $A\beta_{40}$ and PSM $\alpha 3$ of different structures and provided a deeper understanding of the complex interactions between bacterial amyloids and AD-related pathogenic $A\beta$.

Keywords: Alzheimer’s disease; phenol soluble modulins; amyloid β -protein; molecular interactions; molecular dynamics simulation



Citation: Peng, B.; Xu, S.; Liang, Y.; Dong, X.; Sun, Y. Effect of Bacterial Amyloid Protein Phenol–Soluble Modulins Alpha 3 on the Aggregation of Amyloid Beta Protein Associated with Alzheimer’s Disease.

Biomimetics **2023**, *8*, 459.

<https://doi.org/10.3390/biomimetics8060459>

Academic Editor: Jing Sun

Received: 20 August 2023

Revised: 24 September 2023

Accepted: 26 September 2023

Published: 1 October 2023



Copyright: © 2023 by the authors. Licensee MDPI, Basel, Switzerland. This article is an open access article distributed under the terms and conditions of the Creative Commons Attribution (CC BY) license (<https://creativecommons.org/licenses/by/4.0/>).

1. Introduction

Alzheimer’s disease (AD), one of the most common neurodegenerative diseases, is widely recognized as the major cause of dementia. The pathological feature of AD is the plaques formed between neurons in the brain by abnormal levels of the amyloid β -protein ($A\beta$) and the intracellular neurofibrillary tangles caused by the hyperphosphorylation of tau [1–3]. The amyloids cascade hypothesis suggests that $A\beta$ deposition triggers neuronal dysfunction and death in the brain associated with the disease [4]. In recent years, increasing evidence has identified that the gastrointestinal tract and the central nervous system can be bi-directionally linked through the microbiota–gut–brain axis, indicating potentially common pathogenic mechanisms among these diseases. Thus, the intestinal microbiota not only modulates the gastrointestinal tract, but also influences the function and development

of the brain. It has been discovered that gut dysbiosis is linked to neurodegenerative diseases, such as AD, depression, and Parkinson's disease [5–11]. Studies have shown that the interaction of bacterial amyloids produced by intestinal flora and pathogenic amyloids related to neurodegenerative diseases may be one of the main triggers of AD [12,13]. Recent studies on bacterial amyloids have shown that CsgA, the major subunit of bacterial amyloids curli secreted by *Escherichia coli*, could accelerate the formation of A β ₄₀ fibrils in vitro [14]. The FapC amyloid fragment has been shown to accelerate A β aggregation, inducing the neurotoxicity and pathological features of AD [15]. These results demonstrate that bacterial amyloids can interact with pathogenic amyloids, potentially influencing the development of neurodegenerative diseases through a novel mechanism of amyloidosis. However, the specific mechanisms behind the interaction between bacterial amyloids and A β remain elusive and require further exploration.

Phenol-soluble modulins (PSMs) are amphiphilic peptides with a wide range of cytolytic activities, and they serve as an important virulence factor secreted by *Staphylococcus aureus* (*S. aureus*), a representative member of the intestinal flora. The PSM peptides play an important role in stabilizing the biofilm structure by enhancing the biofilm matrix, resisting mechanical stress, and degrading enzyme catabolism [16]. PSM α 3 is the most cytotoxic and soluble of the PSM peptides [17] and has attracted much attention because of its cross- α fibril structure [13]. The unique conformation of PSM α 3 potentiates its toxicity to human cells [18]. The cross- α structure is a newly discovered self-assembly pattern that differs from the typical β -sheet structure. It exhibits an accumulation of α -helix structures perpendicular to the fibril axis (Figure S1) [19]. Previous studies have shown that PSM peptides can selectively cross-seed each other, indicating complex interactions between different PSM peptides [20]. A model has been proposed to describe the complex interaction among various PSM peptides in biofilm formation. The rapidly aggregated PSM α 3 accelerates the assembly of PSM α 1, and PSM α 1 accelerates the aggregation of the remaining PSM peptides [20]. PSM monomers can aggregate into bacterial functional amyloids and cross-seed each other, accelerating the aggregation process. However, the effect of PSM α 3 produced by *S. aureus* with a unique cross- α structure on the aggregation of A β remains poorly understood.

Therefore, the effect of PSM α 3 on the aggregation process of A β ₄₀ was investigated in this study, using various experimental methods such as Thioflavin T (ThT) fluorescence assays, circular dichroism (CD) experiments, and atomic force microscopy (AFM). Moreover, the interaction mechanism between PSM α 3 and A β ₄₀ was analyzed via molecular dynamics (MD) simulations to reveal the influencing mechanism of the intestinal flora on AD at the molecular level.

2. Materials and Methods

2.1. Materials

A β ₄₀ (>95%) was provided by GL Biochem (Shanghai, China). PSM α 3 (>95%) was provided by ZiYu Biotech (Shanghai, China). 1,1,1,3,3,3-Hexafluoro-2-propanol (HFIP) and ThT were provided by Sigma (St. Louis, MO, USA). Antibodies 6E10 and OC were obtained from Covance (Dedham, MA, USA). Secondary antibodies anti-mouse IgG and anti-rabbit IgG were provided by Beyotime (Shanghai, China).

2.2. Preparation of A β ₄₀ and PSM α 3 Monomers

A β ₄₀ was pretreated according to the literature [21]. A β ₄₀ was dissolved in HFIP at a concentration of 1.0 mg/mL and placed stably at 4 °C for 2 h. The solution was then ultrasonicated for 20 min in an ice bath to destroy the A β ₄₀ aggregates. Then, a freeze dryer (FreeZone, Labconco, Kansas City, MI, USA) was used to remove HFIP to obtain fluffy flocculent A β ₄₀, which was stored at -20 °C. PSM α 3 was treated by the same procedure as A β ₄₀ and stored at -20 °C until the beginning of the experiment to ensure PSM α 3 was in a monomeric conformation [21]. For use, A β ₄₀ and PSM α 3 monomers were dissolved in NaOH (20 mM) and ultrasonicated for 5 min, then centrifugated at 16,000 \times g for 20 min at

4 °C. Then, the peptides were diluted to a final concentration of 25 µM with HEPES buffer (30 mM, pH 7.4).

2.3. Preparation of PSMα3 Seeds

The PSMα3 monomer was incubated in an air–bath shaker at 130 rpm and 37 °C for different times (1 to 24 h) and then centrifugated at 16,000× *g* for 20 min at 4 °C. PSMα3 seed suspension was obtained by adding PSMα3 solution into HEPES buffer at a concentration of 5 µM.

2.4. ThT Fluorescence Assay

A 200 µL sample containing Aβ₄₀, PSMα3, and equimolar ThT was mixed evenly and added to 96–well plates at a concentration of 25 µM for both Aβ₄₀ and ThT, and the concentration of PSMα3 seeds was 5 µM. The samples were incubated in a fluorescence plate reader (PerkinElmer, LS55, Waltham, MA, USA) with shaking at 30 min intervals at 37 °C. The ThT emission fluorescence at 480 nm was measured by excitation wavelengths at 440 nm. At least three parallel groups were set up for each experiment and the results were averaged after subtracting the corresponding background.

2.5. AFM Experiments

The Aβ₄₀ monomer (25 µM) solution was cultured with or without the PSMα3 monomer and PSMα3 seeds at 37 °C for 100 h. The 50 µL samples were dropped on a flat mica sheet, and then other impurities were carefully washed away with ultrapure water after 10 min. The morphological characteristics of the samples were observed using atomic force microscopy (CSPM5500, Benyuan, Guangzhou, China). The pixels of the images were set to 1024 × 1024, and at least three separate areas of each sample were scanned by AFM to ensure consistency.

2.6. CD Experiments

The secondary structure of Aβ₄₀ aggregates (25 µM) cultured with or without PSMα3 was examined by a CD spectrometer (J–810, JASCO, Tokyo, Japan). The samples were incubated in an air bath shaker for 100 h and then placed in a quartz cell with a 1 mm optical range. The CD spectra were scanned between 260 nm and 190 nm continuously at 100 nm/min with a bandwidth of 1 nm. The CD spectra were averaged from three parallel samples after subtracting the background.

2.7. Dot–Blot Assays

Ten microliters of Aβ₄₀ (25 µM) co–cultured with or without the PSMα3 monomer and seeds was spotted on a nitrocellulose membrane and dried at room temperature for 1 h. The membrane was blocked with 10% skimmed milk for 1 h. After washing three times with TBS–T buffer (20 mM Tris–HCl, 150 mM NaCl, and 0.05% Tween 20, pH 7.4), the membranes were incubated with the Aβ sequence–specific 6E10 antibody (1:1000) and Aβ fibril–specific OC antibody (1:1000) for 1 h at room temperature and washed three times with TBS–T buffer. The membranes were then incubated with horseradish peroxidase–labeled anti–mouse IgG (1:2000) or anti–rabbit IgG (1:2000) for 1 h at room temperature and washed three times with TBS–T buffer. Finally, color development was performed with an ECL chemiluminescence kit (Beyotime, Shanghai, China). Images were taken using a chemiluminescence imaging system (SH–Compact 523, Shenhua, Hangzhou, China).

2.8. MD Simulations

The structures of Aβ₄₀ (PBD ID: 1BA4) [22] and PSMα3 (PBD ID: 5I55) [19] were selected as the templates. The initial structure of the PSMα3 monomer was taken from a PSMα3 fibrous structure formed by a set of twenty helices (PBD ID: 5I55) [19], and one of the helices was selected as the template. To construct a PSMα3 oligomer model, three

PSM α 3 monomers were placed in parallel with a minimum distance of 1.0 nm to construct an isolated trimeric system [23]. The complex system was formed by docking A β ₄₀ and PSM α 3 using AutoDock Vina [24]. All systems were simulated using the GROMACS 5.1.4 software package [25] with the AMBER 99SB force field [26]. The periodic simulation box was created and the minimum distance from the molecule to the edge of the box was set to 1 nm. The solvent water molecule TIP3P [27] was then filled in the system and Na⁺ and Cl⁻ ions were added to neutralize the electrostatic charges of the simulated systems. The systems were then optimized by energy minimization and performed a solvent equilibrium in 50,000 steps at a constant NVT of 100 ps and 300 K, followed by a pressure equilibrium of 100 ps at NPT conditions. The MD simulations were then performed for 50 ns with a step size of 1 fs. Previous studies have shown that a simulation time of 50 ns is sufficient to bring the complex to equilibrium and to illustrate conformational transitions in peptides [28,29]. The free binding energy between A β ₄₀ and PSM α 3 was calculated by g_mmpbsa [30]. Pymol was used to obtain snapshots. Three independent MD simulations were carried out for each system.

3. Results and Discussion

3.1. Effects of the PSM α 3 Monomer on A β ₄₀ Aggregation

It has been reported that the cross- α structure of PSM α 3 fibrils can specifically bind to the amyloid dye ThT and produce enhanced fluorescence [18]. Here, the aggregation kinetic of PSM α 3 was measured by a ThT fluorescence assay. The aggregation of PSM α 3 was observed as an immediate increase in ThT fluorescence intensity without a significant lag phase. The ThT fluorescence intensity peaked around 2.5 h and then gradually decreased until it reached equilibrium (Figure S2a). The aggregation of PSM α 3 was different from the standard sigmoidal kinetic behavior of A β ₄₀ [31,32], consistent with previous results [20,33]. Studies have shown that newly formed PSM α 3 aggregates are unstable, but they can stabilize the structure by lateral association during aggregation [20]. The CD spectra showed a negative peak at 216 nm (typical β -sheet signal) for A β ₄₀ aggregates, indicative of a β -sheet-rich structure (Figure S2b). In contrast, the CD spectra of PSM α 3 aggregates showed a minimum at 222 nm, implying a reduced helicity of the α -helical structure [34]. Combined with the results of ThT fluorescence experiments in Figure S2a, the above results suggested that PSM α 3 formed the cross- α structure composed of an α -helix, which could bind to the amyloid dye ThT [18]. This is consistent with the results of X-ray diffraction spectroscopy and Fourier transform infrared spectroscopy [19,34].

The morphological characteristics of the A β ₄₀ and PSM α 3 aggregates were examined using AFM. A β ₄₀ formed elongated fibrils after 72 h (Figure S2c), consistent with previous results [35]. However, PSM α 3 formed granular aggregates (Figure S2c), different from the elongated fibril structures reported in the literature [19,34]. This was because differences in experimental conditions, such as peptide concentration, buffer ionic strength, pH, and shaking conditions, can affect the morphology of PSM α 3 aggregates. Overall, these results demonstrate differences in structure and morphology between A β ₄₀ and PSM α 3 aggregates.

To explore whether PSM α 3 plays a role in A β ₄₀ aggregation, the kinetics of A β ₄₀ aggregation cultured with different concentrations of the PSM α 3 monomer was monitored (Figure 1a,b). It can be seen that the maximum ThT fluorescence intensity of A β ₄₀ significantly decreased (Figure 1a), and the lag phase prolonged (Table S1) with increasing the concentration of the PSM α 3 monomer. The kinetic curves of 0 to 20 h in Figure 1a are magnified in Figure 1b, allowing a clearer observation of the short time changes in the ThT fluorescence intensity. Interestingly, when A β ₄₀: PSM α 3 > 1:1, the aggregation of A β ₄₀ still followed the sigmoidal kinetic curve with reduced ThT fluorescence. The aggregation of A β ₄₀ appeared to be completely inhibited by the addition of equal concentrations of the PSM α 3 monomer (purple line in Figure 1a). However, when A β ₄₀: PSM α 3 < 1:1, the aggregation kinetics of A β ₄₀ no longer fitted the typical sigmoidal curve but tended to follow the aggregation kinetics of PSM α 3 itself (green and blue lines in Figure 1a). This

indicates that the ratio of $A\beta_{40}$ to $PSM\alpha 3$ monomer influenced the type of aggregation. The amyloids with a higher amount than the other in the mixture dominated the aggregation dynamics and determined the amyloids aggregation pathway. To further explore the mechanism of inhibition, the relevant kinetic parameters, including k_1k_+ (related to the primary pathway) and k_2k_+ (related to the secondary pathway), were calculated using the Amylofit program [36]. The results revealed that both the k_1k_+ and k_2k_+ values decreased in the presence of the $PSM\alpha 3$ monomer, while the k_2k_+ value decreased more significantly (Figure S3a). It indicated that the $PSM\alpha 3$ monomer mainly inhibited the secondary pathway of unseeded $A\beta_{40}$ aggregation.

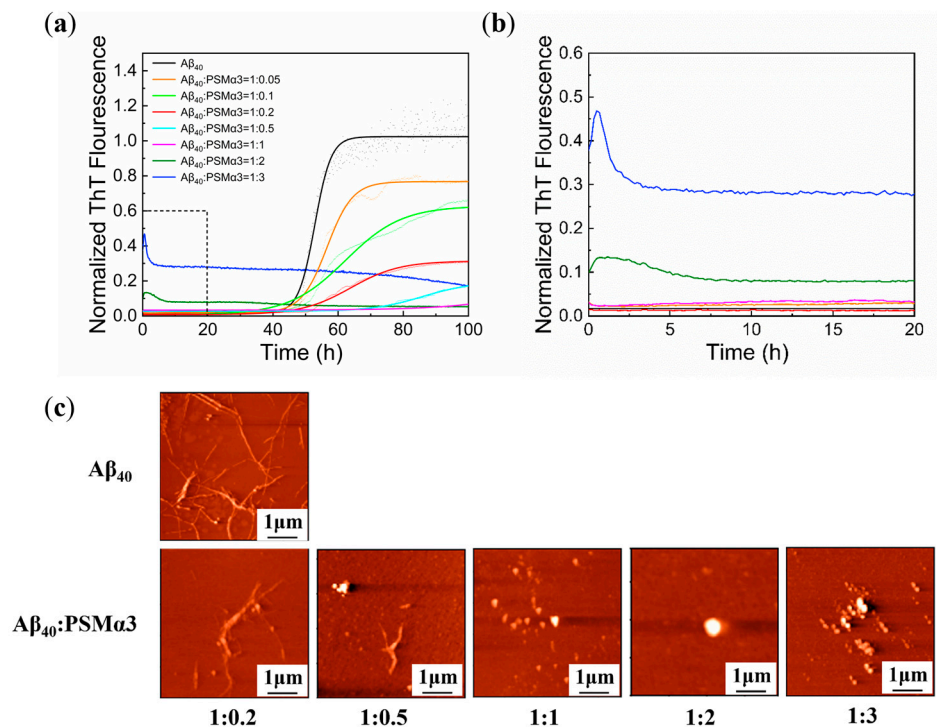


Figure 1. Effect of the $PSM\alpha 3$ monomer on $A\beta_{40}$ aggregation: (a) aggregation kinetics of $A\beta_{40}$ (25 μ M) cultured with or without the $PSM\alpha 3$ monomer at different concentrations measured by ThT fluorescence assay; (b) the enlarged version of the dotted frame area in (a); (c) AFM images of $A\beta_{40}$ aggregates cultured with or without the $PSM\alpha 3$ monomer of different concentrations at 37 $^{\circ}$ C for 100 h.

The morphology of $A\beta_{40}$ incubated with different concentrations of the $PSM\alpha 3$ monomer is shown in Figure 1c. When $A\beta_{40}$: $PSM\alpha 3 > 1:1$, the total density of fibrils detected by AFM decreased and gradually transformed into sparse short fibrils or some granular aggregates. When $A\beta_{40}$: $PSM\alpha 3 < 1:1$, no fibrous structures can be observed (Figure 1c). This is consistent with the ThT fluorescence assay (Figure 1a), indicating that the $PSM\alpha 3$ monomer inhibited the aggregation of $A\beta_{40}$ in a concentration–dependent manner and could change the aggregation pathway of $A\beta_{40}$.

The inhibitory effect of the $PSM\alpha 3$ monomer on $A\beta_{40}$ aggregation was further demonstrated by dot–blot assays with antibody 6E10 ($A\beta_{1-16}$ sequence–specific) and antibody OC (fibril–specific) (Figure S4). The 6E10 antibody recognizes the $A\beta_{1-16}$ sequence, and all of the $A\beta$ species can be stained by it [37]. By staining with 6E10, there was no change in spot size or darkness in any $A\beta$ or $A\beta$ – $PSM\alpha 3$ species at 0 h and 100 h, indicating the stable presence of $A\beta$ during incubation (Figure S4a). At the beginning of incubation (0 h), $A\beta$ fibrils were rarely detected by antibody OC in the presence or absence of the $PSM\alpha 3$ monomer (Figure S4b, left). The OC–positive dots were detected in $A\beta_{40}$ only after 100 h of incubation, indicating the formation of a large number of $A\beta$ fibrils, consistent with the previous results [38]. However, after co–cultivation with the $PSM\alpha 3$ monomer, the positive response was significantly reduced by increasing the $PSM\alpha 3$ concen-

tration (Figure S4b, right), indicating that the PSM α 3 monomer significantly inhibited the formation of A β ₄₀ fibrils, which was in agreement with the ThT and AFM results (Figure 1).

According to the above results, it can be concluded that the cross–interaction between the PSM α 3 monomer and the A β ₄₀ monomer resulted in the formation of non–fibrillar heterogeneous aggregates (Figure 1c), similar to the hetero–oligomers formed by A β and human islet amyloid polypeptide (hIAPP) [39,40] or tau [41]. These heterogeneous structures interfered with the conformational transitions of A β ₄₀, resulting in reduced ThT fluorescence (Figure 1a). Moreover, A β ₄₀ and PSM α 3 monomers were reported to retain α –helix and disordered structures during the initial stages of aggregation [19,22]. The diversity and instability of structures hindered their common nucleation process, resulting in difficult cross–seeding with each other, and thus leading to an increased lag phase [42].

3.2. Effect of PSM α 3 Seeds on A β ₄₀ Aggregation

The secondary nucleation mechanism of A β suggests that preformed fibril seeds of A β could accelerate its aggregation process [43]. In addition, several different disease–associated misfolded proteins, such as hIAPP [44], tau [45], and α –synuclein [46], could also hybridize with A β and promote amyloids formation. Studies have shown that the main molecular mechanism for the formation of PSM peptides was secondary nucleation with selective cross–seeding ability [20]. To investigate whether PSM α 3 seeds accelerate A β aggregation through cross–seeding, thereby aggravating AD, cross–seeding experiments were performed using 20% preformed PSM α 3 seeds added to the A β ₄₀ monomer. It was observed that the aggregation of A β ₄₀ incubated with PSM α 3 seeds fitted the sigmoidal kinetic curve with no significant change in the maximum ThT fluorescence intensity (Figure 2a). The results indicated that the PSM α 3 seeds had weak effects on the aggregation pathway and the formation of the β –sheet structure of A β ₄₀. However, compared to the non–seeded aggregation, the lag phase of A β ₄₀ incubated with PSM α 3 seeds significantly decreased (Table S2). The aggregation of A β ₄₀ incubated with PSM α 3 seeds cultured for 2.5 h showed the shortest lag phase (~33.8 h), indicating that the PSM α 3 seeds cultured for 2.5 h showed the most significant promotion effect on A β ₄₀ aggregation. This might be because the ThT fluorescence intensity peaked at 2.5 h in the aggregation kinetic curve of PSM α 3 (Figure S2a), indicating that PSM α 3 contained the highest content of the cross– α structure after 2.5 h of aggregation. A kinetic analysis revealed a significant increase in $k_n k_+$ and a slight decrease in $k_2 k_+$ in the presence of the PSM α 3 seeds (Figure S3b). Similarly, the PSM α 3 seeds at 2.5 h showed the highest $k_n k_+$ value, in agreement with the lag phase results (Table S2). These results confirmed that the PSM α 3 seeds decreased the lag phase of A β ₄₀ by promoting the primary pathway, which was different from the role of the PSM α 3 monomer (Figure 1a). This may be due to the fact that the PSM α 3 seeds were formed by the cross– α structures, which were highly similar to the β –sheet structures [19]. The PSM α 3 seeds could serve as templates to facilitate cross–seeding and promote the formation of β –sheet structures, thus accelerating the aggregation of A β ₄₀ [47]. Meanwhile, the promotion effect of the PSM α 3 seeds on A β ₄₀ aggregation was correlated with the content of the cross– α structure. The higher content of the cross– α structure, the more obvious the promotion effect of the PSM α 3 seeds.

To investigate the effect of the PSM α 3 seeds on the secondary structure of A β ₄₀, the CD spectra of A β ₄₀ induced by the PSM α 3 seeds were recorded (Figure 2b). They showed a minimum at approximately 216 nm, and the peak intensity was close to that of A β ₄₀ cultured alone (Figure 2b). The contents of different secondary structures were calculated from the CD spectrum (Table 1), and it was observed that the content of α –helix structures slightly increased after co–culture with the PSM α 3 seeds. This might be because the main secondary structure of the PSM α 3 aggregates is α –helix [34] (Figure S2b), thus increasing the content of the α –helix structure in the mixed system. In contrast, the changes in the content of the β –sheet structure were not obvious (~70%) (Table 1), indicating that the PSM α 3 seeds had little effect on the content of the β –sheet structure in the A β ₄₀ aggregates. But compared with the PSM α 3 seeds of other incubation times, the cross–seeding of A β ₄₀ and PSM α 3 seeds at 2.5 h had the highest content of α –helix structures (29.3%) and

the lowest content of β -sheet structures (63.6%). This also indicated that PSM α 3 seeds cultured for 2.5 h contained the highest content of cross- α , consistent with the aggregation kinetics of PSM α 3 (Figure S2a). Their interaction with A β ₄₀ had the most significant impact, which affected the conformational transitions of A β ₄₀, increased the content of the α -helix structure, and decreased the content of the β -sheet structure. Further observation of the aggregate morphology showed that A β ₄₀ induced by PSM α 3 seeds forms more fibrils than A β ₄₀ alone, indicating that the PSM α 3 seeds promoted the formation of A β ₄₀ fibrils. Dot-blot assays also showed that A β ₄₀ co-cultured with PSM α 3 seeds exhibited significant OC-positive dots unaffected by increasing the incubation time with the PSM α 3 seeds, indicating the substantial formation of A β fibrils (Figure S5), consistent with the results of ThT and AFM experiments (Figure 2).

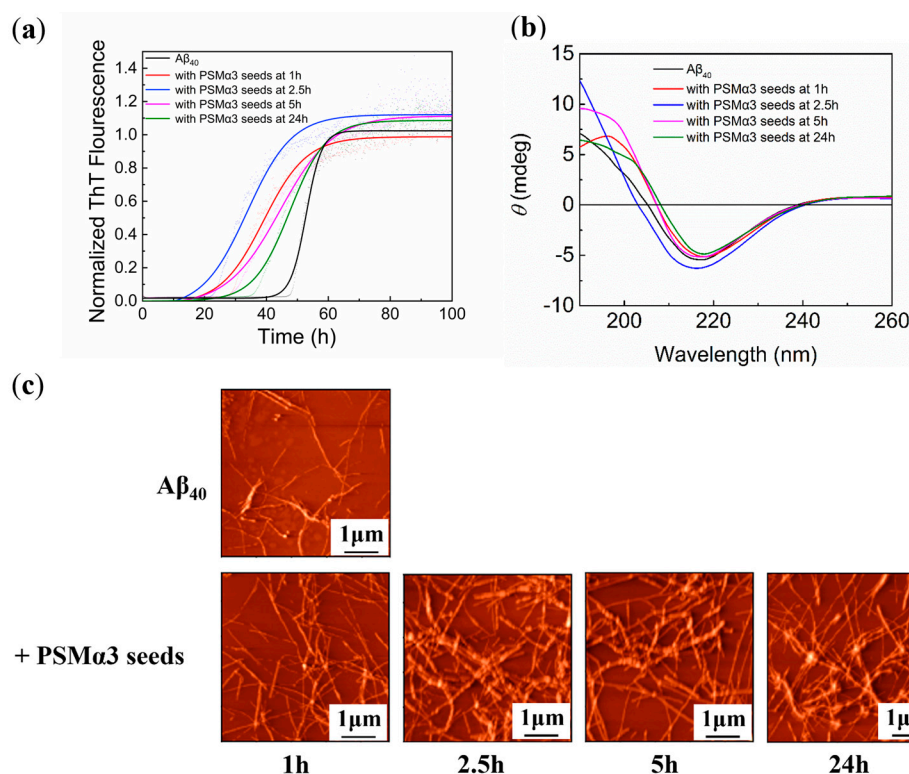


Figure 2. Effect of PSM α 3 seeds on A β ₄₀ aggregation: (a) aggregation kinetics of A β ₄₀ (25 μ M) cultured without or with PSM α 3 seeds (5 μ M) at 1 h, 2.5 h, 5 h, and 24 h measured by ThT fluorescence assays for 100 h; (b) CD spectra of A β ₄₀ aggregates cultured with or without PSM α 3 seeds at 1 h, 2.5 h, 5 h, and 24 h for 100 h; (c) AFM images of A β ₄₀ cultured with or without PSM α 3 seeds at 37 $^{\circ}$ C for 100 h.

Table 1. Secondary structure distributions of A β ₄₀ aggregates incubated with PSM α 3 seeds of different culture times calculated from the CD spectrum.

Sample (%)	α -Helix	β -Sheet	Turn	Others
A β ₄₀	10	74.4	3.8	11.8
with PSM α 3 seeds at 1 h	7.8	73.2	1.2	17.9
with PSM α 3 seeds at 2.5 h	29.3	63.6	7.1	0
with PSM α 3 seeds at 5 h	14.2	81.9	3.8	0
with PSM α 3 seeds at 24 h	18.3	79.1	2.6	0

3.3. Molecular Docking of PSM α 3 and A β ₄₀ Monomer

To analyze the PSM α 3 monomer (PSM α 3m) and oligomer (PSM α 3o) binding to A β ₄₀ at the molecular level, the corresponding composite models were constructed by docking the PSM α 3m (PDB ID: 5I55) [19] or the PSM α 3o with the A β ₄₀ monomer (PDB ID:

1BA4) [22] using AutoDock Vina. The docking results demonstrated that the best binding conformation of the $A\beta_{40}$ –PSM α 3m complex had a binding free energy of -6.2 kcal/mol in the top 10 binding conformations (Table S3), similar to the binding energies of $A\beta$ and other amyloids, such as $A\beta$ and the hIAPP monomer (~ -6.4 kcal/mol) [48,49]. In contrast, the best binding conformation of the $A\beta_{40}$ –PSM α 3o complex had a binding free energy of -13.0 kcal/mol (Table S4), over 2.1-fold higher than that of the $A\beta_{40}$ –PSM α 3m complex, implying that the PSM α 3o binds to the $A\beta_{40}$ monomer to form a more stable complex than the PSM α 3m. This might be because the $A\beta_{40}$ monomer and the PSM α 3m are mostly in α -helix and disordered conformations [36]; the structural disorder and dynamic instability led to difficulties in their binding. However, the PSM α 3o formed a stable cross- α structure [23], which facilitated a more stable binding to the $A\beta_{40}$ monomer.

3.4. MD Simulations on PSM α 3 and $A\beta_{40}$ Monomers and Their Complex

To investigate the effects of the PSM α 3m on the conformational transitions of $A\beta_{40}$, the optimal conformation of the $A\beta_{40}$ –PSM α 3m complex was selected as the initial conformation, and 50 ns MD simulations were performed with $A\beta_{40}$ or the PSM α 3m alone as the control for comparison. The root mean square deviation (RMSD) was calculated first to assess the stability of the simulated systems. As shown in the RMSD plots (Figure 3a), the RMSD values of all three systems initially increased rapidly and then stabilized after 30 ns at around 0.4 nm, 0.8 nm, and 0.9 nm, respectively, indicating that all three systems reached equilibrium within 20 ns. It can be seen that the initial equilibrium speed of the $A\beta_{40}$ –PSM α 3m complex was slower than that of $A\beta_{40}$ alone, and its RMSD value was higher than that of $A\beta_{40}$ alone. These results indicate that the PSM α 3m affected the conformational changes of $A\beta_{40}$ in the initial stage of the simulations and reduced system stability.

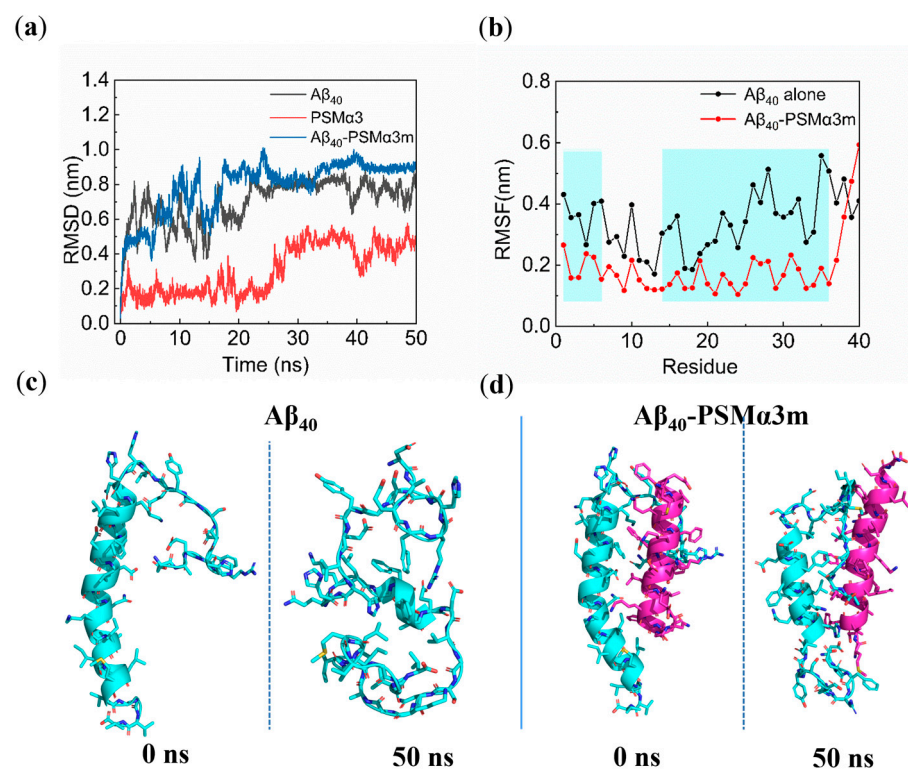


Figure 3. MD simulations of the PSM α 3 monomer (PSM α 3m) and the $A\beta_{40}$ monomer and their complex: (a) RMSD of $A\beta_{40}$, PSM α 3, and $A\beta_{40}$ –PSM α 3m complex; (b) RMSF of each residue of $A\beta_{40}$ without or with PSM α 3m; (c,d) initial (0 ns) and equilibrium (50 ns) states of (c) $A\beta_{40}$ and (d) $A\beta_{40}$ –PSM α 3m complex. Blue and purple represent the $A\beta_{40}$ monomer and PSM α 3m, respectively.

To identify the key residues during the interaction between the PSM α 3m and the A β ₄₀ monomer, the root mean square fluctuation (RMSF) of residues in the last 20 ns of the MD simulations was calculated. It was found that the RMSF values of A β ₄₀ residues in the A β ₄₀–PSM α 3m complex were generally smaller than that of A β ₄₀ alone (Figure 3b), indicating that the tight binding of the PSM α 3m reduced the flexibility of residue fluctuations of A β ₄₀. Moreover, the fluctuations of the Asp1–His6 and His14–Val36 regions in A β ₄₀ significantly decreased by the presence of the PSM α 3m, indicating that the PSM α 3m exhibits a stronger impact on these regions. These results suggested that the PSM α 3m tightly bound the Asp1–His6 and His14–Val36 regions in A β ₄₀ and exhibited a disruptive effect on the Asp23–Lys28 salt bridge in A β ₄₀. Hydrophobic interactions and the salt bridge have been reported to play a critical role in stabilizing the structure of A β fibrils [50]. The disruption of the salt bridge prevented the formation of the β –sheet structure, thus reducing the structural stability of A β ₄₀ [51].

Furthermore, other structural parameters of different systems were analyzed to estimate the fast conformational transitions of A β ₄₀. The results showed that the binding of the PSM α 3m increased the radius of gyration (R_g) and the solvent–accessible surface area (SASA) of A β ₄₀ (Table S5), indicating that the PSM α 3m changed the conformational denseness of A β ₄₀ and increased the exposure of the contact area to the solvent, thus destabilizing the system, consistent with the RMSD results (Figure 3a). In addition, the PSM α 3m reduced the number of intramolecular hydrogen bonds (H–bonds) of A β ₄₀ (Table S5), which was detrimental to maintaining the structural stability of A β ₄₀ [52].

To observe the effect of the PSM α 3m on the structure of the A β ₄₀ monomer, snapshots of A β ₄₀ and the A β ₄₀–PSM α 3m complex in the initial and equilibrium states were extracted (Figure 3c,d). The conformational transitions from the initial α –helix structure to a random coil structure were observed in the A β ₄₀ monomer, which is a critical step in forming a highly ordered β –sheet structure for A β aggregation [53]. However, the α –helix structure of A β ₄₀ in the A β ₄₀–PSM α 3m complex was well preserved (Figure 3d), indicating that the PSM α 3m inhibited the conformational transitions of the A β ₄₀ monomer.

The content of secondary structures in the equilibrium state showed that A β ₄₀ alone contained only 13.8% of the α –helix structure and 4.5% of the β –bridge structure (Table S6), which was a transition structure that transformed into the β –sheet structure [54]. The results indicate that the A β ₄₀ monomer transformed from the α –helix to the coil structure, and then formed the β –sheet structure, which is consistent with previous studies [55,56]. However, the binding of the PSM α 3m resulted in a higher content of the α –helix structure (36.3%) than that of A β ₄₀ alone, accompanied by a decrease in the content of coil (29.1%) and turn structures (24.1%), and the β –bridge structure was not formed (Table S6). These results showed that the PSM α 3m inhibited the conformational transitions of A β ₄₀ from the α –helix structure to coil and turn structures, thus suppressing the formation of β –sheet structures, which prolonged the lag phase of A β ₄₀ and inhibited the fibrillization of A β ₄₀ (Figure 1a and Table S1).

To demonstrate how the PSM α 3m inhibits the conformational transitions of A β ₄₀, we investigated the changes in secondary structure during the whole MD simulation. For A β ₄₀ alone, the α –helix structures in the Gln15–Ala30 region were rapidly transformed into the coil and turn structures after 20 ns, and the β –bridge was formed in the Phe4–Ser8 region after 40 ns (Figure S6a), consistent with the previous findings [55,56]. In contrast, the Gln15–Asp23 regions maintained their initial α –helix structure during the 50 ns MD simulation in the A β ₄₀–PSM α 3m system. The regions of Val12–Gln15, which had the coil structure in the initial state, transformed into α –helix after 10 ns (Figure S6b). Moreover, no β –sheet or β –bridge structures were detected during the whole 50 ns MD simulations. It is known that the maintenance of the α –helix structure inhibits the aggregation of A β into toxic oligomers [57]. Therefore, the PSM α 3m inhibited A β ₄₀ aggregation by stabilizing the formation of α –helix structures and suppressing the generation of β –sheet structures.

To further investigate the intermolecular interactions between the PSM α 3m and the A β ₄₀ monomer, the binding free energy between the PSM α 3m and the A β ₄₀ monomer was

calculated. The simulated trajectory of the last 20 ns was collected and calculated by the molecular mechanic Poisson–Boltzmann surface area (MM–PBSA) method [30]. The binding free energy between the PSM α 3m and the A β ₄₀ monomer was -270.7 kJ/mol (Table S7), indicating a high affinity of the PSM α 3m and the A β ₄₀ monomer [48,49]. An analysis of the contribution of each energy component showed that van der Waals hydrophobic energy ($\Delta G_{\text{vdw}} = -373.5$ kJ/mol) and electrostatic energy ($\Delta G_{\text{elec}} = -963.9$ kJ/mol) were contributing more to the binding than other energies (Table S7), indicating that hydrophobic and electrostatic interactions play a critical role in the binding of the PSM α 3m to the A β ₄₀ monomer. The free energy was decomposed to search for the key residues in the interaction between the PSM α 3m and the A β ₄₀ monomer. As shown in Figure 4, Asp1 and Leu17 of A β ₄₀ and Met1, Glu2, Phe3, Leu7, Leu14, and Phe18 of the PSM α 3m contributed greatly to the binding of the PSM α 3m to the A β ₄₀ monomer (binding free energy < -15.0 kJ/mol), in which the van der Waals force and electrostatic interactions were the main contributors (Table S8).

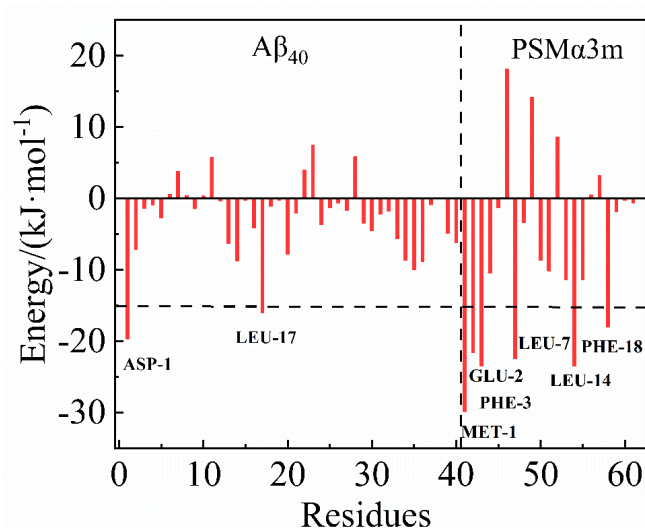


Figure 4. Energy decomposition diagram of each amino acid residue in the A β ₄₀–PSM α 3m complex.

It is known that the aggregation of A β is mainly controlled by hydrophobic interactions and H–bonding [58]. Six H–bonds were observed between the A β ₄₀ monomer and the PSM α 3m, which were mainly located at the N–terminal of A β ₄₀ (Figure S7a). It has been reported that the flexibility of the N–terminal plays a significant role in the aggregation and toxicity of A β [59]. This implies that the PSM α 3m could alter the aggregation tendency of A β ₄₀ by decreasing the flexibility of the N–terminal. Moreover, the A β ₄₀ monomer is negatively charged [22], while the PSM α 3m is positively charged [19]. The opposite charges lead to strong electrostatic interactions between A β ₄₀ and the PSM α 3m, which facilitated their stable binding. In addition, some hydrophobic residues (Met1, Phe3, Leu7, Leu14, and Phe18) of the PSM α 3m could provide hydrophobic interactions with the A β ₄₀ monomer. Therefore, the hydrophobic and electrostatic interactions between the PSM α 3m and the A β ₄₀ monomer promote the tight binding and inhibit the conformational transitions of the A β ₄₀ monomer.

3.5. MD Simulations on Interactions between PSM α 3 Oligomer and A β ₄₀ Monomer

To examine the effect of the PSM α 3o on the conformational transitions of the A β ₄₀ monomer, the interaction of the PSM α 3o with the A β ₄₀ monomer was analyzed using MD simulations (Figure 5). The RMSD value of the PSM α 3o–A β ₄₀ system was stabilized at around 0.8 nm after 40 ns, indicating that the system reached equilibrium thereafter (Figure 5a). Similar to the PSM α 3m, the PSM α 3o increased R_g and SASA values and decreased the number of intramolecular H–bonds of the A β ₄₀ monomer (Table S5), making the whole system unstable, and the RMSD values increased (Figure 5a). The RMSF value of the N–terminal residues of A β ₄₀ increased (Figure 5b), indicating that

the PSM α 3o increases the N-terminal flexibility of A β ₄₀ to accelerate the conformational transitions of A β ₄₀ [59]. Moreover, the PSM α 3o significantly decreased the RMSF value of the Tyr10–Val40 region in A β ₄₀ (Figure 5b), indicating that the PSM α 3o mainly interacted with this region and suppressed the dynamic fluctuation of the residues.

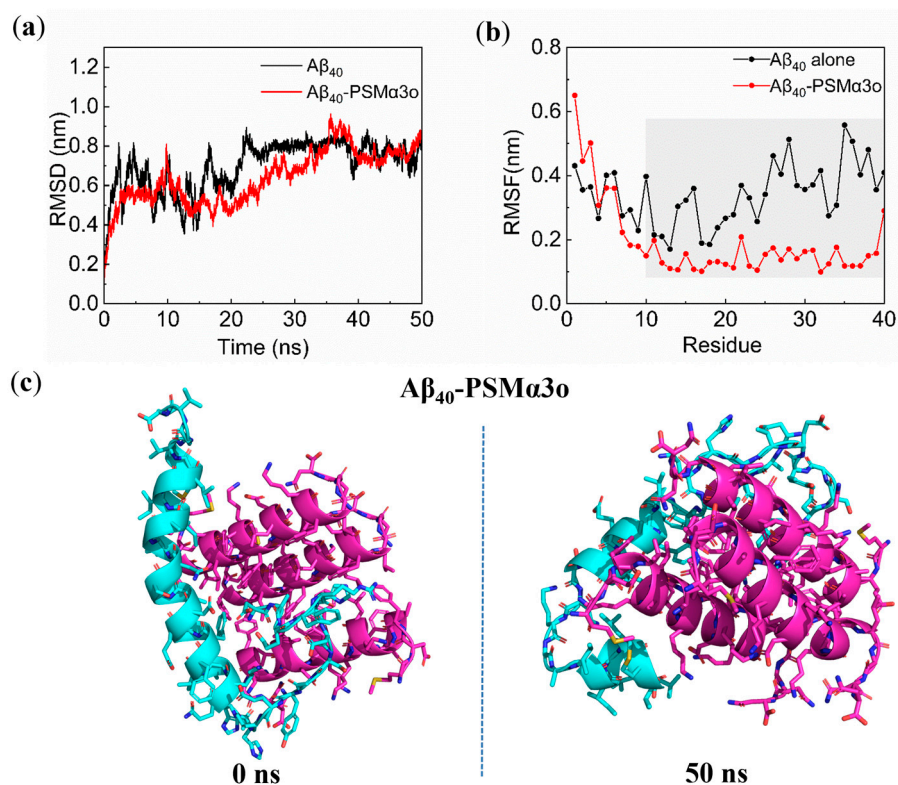


Figure 5. MD simulations of A β ₄₀–PSM α 3 oligomer (PSM α 3o) complex: (a) RMSD of A β ₄₀ and A β ₄₀–PSM α 3o system; (b) RMSF of each amino acid residue of A β ₄₀ without or with PSM α 3o; (c) initial (0 ns) and equilibrium (50 ns) states of the A β ₄₀–PSM α 3o system. Blue and purple represent the A β ₄₀ monomer and PSM α 3o, respectively.

Notably, the A β ₄₀–PSM α 3o complex at the equilibrium state (50 ns) formed a characteristic turn-like structure in A β ₄₀ (Figure 5c), which was different from the A β ₄₀–PSM α 3m system (Figure 3d). It is known that this turn-like structure stabilizes the β -turn- β structure and promotes the formation of the folding core for A β fibrillation [36,60]. From the content of secondary structures at equilibrium, it was found that the β -bridge structure (0.5%) was still present in the A β ₄₀–PSM α 3o system (Table S6), which was formed in the Phe4–Ser8 region of A β ₄₀ (Figure S6c), indicating that the PSM α 3o could not inhibit the formation of the β -sheet structures in A β ₄₀. This is consistent with the results of the ThT fluorescence and CD experiments (Figure 2a and Table 1), as the PSM α 3o did not significantly affect the maximum ThT fluorescence intensity or the content of the β -sheet structure of A β ₄₀, which also suggested that the PSM α 3o weakly affected the conformational transitions of the A β ₄₀ monomer. Furthermore, the MM–PBSA results showed that the binding energy of the PSM α 3o to the A β ₄₀ monomer was -135.5 kJ/mol, significantly lower than the PSM α 3m to the A β ₄₀ monomer (-270.7 kJ/mol) (Table S7). This is mainly due to the significantly weaker van der Waals hydrophobic energy between A β ₄₀ and the PSM α 3o (-251.0 kJ/mol) than the PSM α 3m (-373.5 kJ/mol). Free energy decomposition showed that the PSM α 3o mainly combined with the central hydrophobic core (CHC) and the C-terminal region of A β ₄₀ (His13–Val36) (Figure 6a), which plays a decisive role in the A β oligomerization [50]. It can be found that some hydrophobic residues (Leu7, Phe10, and Phe18) of the PSM α 3o contributed significantly to the high binding energy, although their contribution was generally lower than that of the PSM α 3m (Figure 6b). In addition, only one stable H-bond was observed in

the A β ₄₀–PSM α 3o complex (Figure S7b), indicating that the H–bonding between the A β ₄₀ monomer and the PSM α 3o was much weaker than for the PSM α 3m. These results suggest that the weaker H–bonding and hydrophobic interactions resulted in a lower binding energy of the PSM α 3o to the A β ₄₀ monomer than that of the PSM α 3m, leading to the weak effect of the PSM α 3o on the conformational transitions of A β ₄₀.

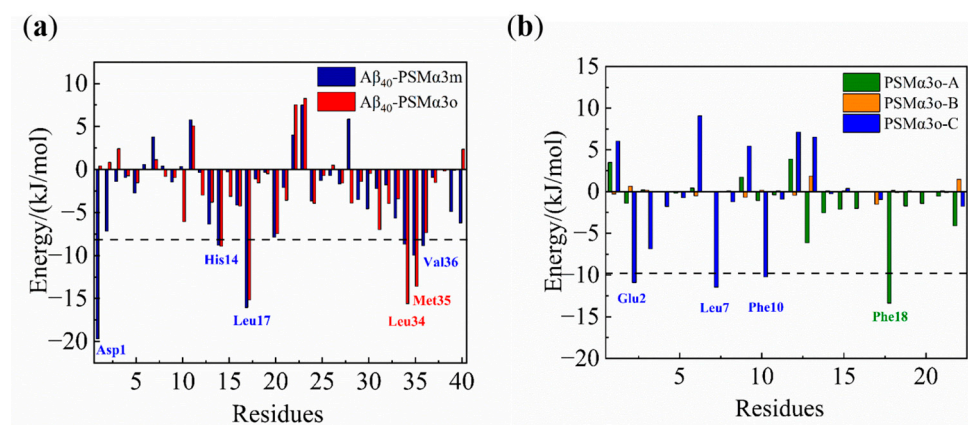


Figure 6. Energy decomposition diagram of each residue of (a) A β ₄₀ and (b) PSM α 3o. Blue and red represent residues of A β ₄₀ in the A β ₄₀–PSM α 3m and A β ₄₀–PSM α 3o complexes, respectively. Green, yellow and blue separately represent the three chains of PSM α 3o.

According to the above studies, it may be concluded that electrostatic and hydrophobic interactions contributed to the binding of the PSM α 3m to the A β ₄₀ monomer. PSM α 3m had a high binding affinity for the A β ₄₀ monomer, with a total of six H–bonds formed between the two monomers, and some hydrophobic residues (Met1, Phe3, Leu7, Leu14, and Phe18) of the PSM α 3m provided hydrophobic interactions with A β ₄₀. The hydrophobic interactions and H–bonding led to the tight binding of the PSM α 3m to the A β ₄₀ monomer and inhibited the conformational transitions of A β ₄₀ from the α –helix to β –sheet structure. In contrast, the PSM α 3o only formed one stable H–bond with the A β ₄₀ monomer, and the weaker H–bonding and hydrophobic interactions resulted in a lower binding free energy of the PSM α 3o to the A β ₄₀ monomer, leading to the small role of the PSM α 3o in inhibiting the formation of the β –sheet structure in A β ₄₀.

4. Conclusions

We have explored the effect of PSM α 3, a bacterial amyloid with a unique cross– α structure, on the aggregation kinetics, molecular structures, and conformational transitions of the A β ₄₀ monomer using experimental and computational approaches. The results showed that the PSM α 3 monomer inhibits A β ₄₀ aggregation in a concentration–dependent manner, prolongs its aggregation lag phase, and redirects the aggregation pathway of A β ₄₀ to form granular structures. In contrast, the PSM α 3 oligomer promotes the generation of the β –sheet structure and shortens the lag phase of A β ₄₀ aggregation. The cross– α structure of PSM α 3 plays an important role in the aggregation of A β ₄₀. The higher the cross– α content of PSM α 3, the more obvious the promotion effect on the aggregation of A β ₄₀. MD simulations further support these observations and identify the key regions and amino acid residues of A β ₄₀ and PSM α 3 in the interactions. The PSM α 3 monomer binds to the Asp1–Ala2 and His13–Val36 regions in the A β ₄₀ monomer via hydrophobic and electrostatic interactions, which prevents the conformational transitions of A β ₄₀ from the initial α –helix structure to the β –sheet structure. In contrast, the PSM α 3 oligomer mainly binds to the CHC and the C–terminal region of the A β ₄₀ monomer through weak H–bonding and hydrophobic interactions, resulting in a weak role in the conformational transitions of A β ₄₀. This work reveals different interactions between PSM α 3 and A β ₄₀, providing deeper insights into the complex interactions between bacterial amyloids and AD–associated pathogenic A β .

Since the formation of cross- α fibrils by PSM α 3 enhances the toxicity to human cells [18] and promotes the formation of the β -sheet structures of A β ₄₀, subsequent studies should direct towards examining the co-aggregation of PSM α 3 and A β ₄₀ in vivo. In addition, it has been shown that some amyloid-derived fragments with cross-seeding capacity can bind to amyloids and inhibit its aggregation [61,62]. The PSM α 3 monomer has a strong affinity for A β ₄₀ and can significantly inhibit the formation of the β -sheet structure, and its derived fragments may serve as potential inhibitors of A β aggregation in vivo. The new findings may provide molecular insights into a potential association between AD and the intestinal flora and provide a potential strategy for the design of amyloids inhibitors based on cross-seeding.

Supplementary Materials: The following supporting information can be downloaded at: <https://www.mdpi.com/article/10.3390/biomimetics8060459/s1>, Table S1: Maximum ThT fluorescence intensity (y_{\max}) and lag phase time (T_{lag}) of aggregation kinetics of A β ₄₀ (25 μ M) with different concentrations of the PSM α 3 monomer; Table S2: Maximum ThT fluorescence intensity (y_{\max}) and lag phase time (T_{lag}) of aggregation kinetics of A β ₄₀ (25 μ M) incubated without or with PSM α 3 seeds; Table S3: Top 10 binding energies of the PSM α 3m–A β ₄₀ complex calculated by molecular docking using Autodock Vina; Table S4: Top 10 binding energies of PSM α 3o and A β ₄₀ calculated by molecular docking using Autodock Vina; Table S5: Structural parameters of the A β ₄₀ monomer in different systems in the equilibrium state; Table S6: Secondary structure composition of the A β ₄₀ monomer in different systems in the equilibrium state; Table S7: Binding free energy components of the A β ₄₀–PSM α 3m and A β ₄₀–PSM α 3o systems calculated using the MM–PBSA method; Table S8: Energy components of key residues of A β ₄₀–PSM α 3m system; Figure S1: Crystal structure of PSM α 3 (PDB ID: 5I55); Figure S2: Aggregation kinetics of PSM α 3; Figure S3: Relative kinetic rate constants of A β ₄₀ aggregation in the presence of the PSM α 3 monomer or PSM α 3 seeds; Figure S4: Effects of the PSM α 3 monomer at different concentrations on the formation of A β ₄₀ (25 μ M) fibrils at 0 h and 100 h; Figure S5: Effects of PSM α 3 seeds (5 μ M) at 1 h, 2.5 h, and 24 h on the formation of A β ₄₀ (25 μ M) fibrils at 0 h and 100 h; Figure S6: The secondary structure components of A β ₄₀ during the 50 ns MD simulations in A β ₄₀ only, A β ₄₀–PSM α 3m, and A β ₄₀–PSM α 3o systems; Figure S7: H–bonds between the A β ₄₀ monomer and PSM α 3m or PSM α 3o. Reference [63] is cited in the supplementary materials.

Author Contributions: Conceptualization, X.D. and Y.S.; formal analysis, B.P. and Y.L.; funding acquisition, X.D. and Y.S.; investigation, B.P. and Y.L.; writing—original draft, B.P. and S.X.; writing—review and editing, B.P., S.X., X.D. and Y.S. All authors have read and agreed to the published version of the manuscript.

Funding: This work was funded by the National Natural Science Foundation of China (no. 21978207).

Institutional Review Board Statement: Not applicable.

Data Availability Statement: Not applicable.

Conflicts of Interest: The authors declare no conflict of interest.

References

1. Long, J.M.; Holtzman, D.M. Alzheimer disease: An update on pathobiology and treatment strategies. *Cell* **2019**, *179*, 312–339. [[CrossRef](#)] [[PubMed](#)]
2. Zhang, H.; Ng, K.P.; Therriault, J.; Kang, M.S.; Pascoal, T.A.; Rosa-Neto, P.; Gauthier, S. Cerebrospinal fluid phosphorylated tau, visinin-like protein-1, and chitinase-3-like protein 1 in mild cognitive impairment and Alzheimer’s disease. *Transl. Neurodegener.* **2018**, *7*, 23. [[CrossRef](#)] [[PubMed](#)]
3. D’Arrigo, J.S. Targeting early dementia: Using lipid cubic phase nanocarriers to cross the blood-brain barrier. *Biomimetics* **2018**, *3*, 4. [[CrossRef](#)] [[PubMed](#)]
4. Karran, E.; Mercken, M.; De Strooper, B. The amyloid cascade hypothesis for Alzheimer’s disease: An appraisal for the development of therapeutics. *Nat. Rev. Drug Discov.* **2011**, *10*, 698–712. [[CrossRef](#)]
5. Du, X.G.; Wang, X.Y.; Geng, M.Y. Alzheimer’s disease hypothesis and related therapies. *Transl. Neurodegener.* **2018**, *7*, 2. [[CrossRef](#)]
6. Jiang, C.M.; Huang, P.R.; Liu, Z.; Zhao, B. The gut microbiota and Alzheimer’s disease. *Alzheimers Dis.* **2017**, *58*, 1–15. [[CrossRef](#)]
7. Feng, M.; Hou, T.S.; Zhou, M.Z.; Cen, Q.Y.; Yi, T.; Bai, J.F.; Zeng, Y.; Liu, Q.; Zhang, C.S.; Zhang, Y.J. Gut microbiota may be involved in Alzheimer’s disease pathology by dysregulating pyrimidine metabolism in APP/PS1 mice. *Front. Aging Neurosci.* **2022**, *14*, 967747. [[CrossRef](#)]
8. Szablewski, L. Human gut microbiota in health and Alzheimer’s disease. *Alzheimers Dis.* **2018**, *62*, 549–559. [[CrossRef](#)]

9. Chandra, S.; Alam, M.T.; Dey, J.; Sasidharan, B.C.P.; Ray, U.; Srivastava, A.K.; Gandhi, S.; Tripathi, P.P. Healthy gut, healthy brain: The gut microbiome in neurodegenerative disorders. *Curr. Top. Med. Chem.* **2020**, *20*, 1142–1153. [[CrossRef](#)]
10. Cryan, J.F.; O’Riordan, K.J.; Cowan, C.S.M.; Sandhu, K.V.; Bastiaanssen, T.F.S.; Boehme, M.; Codagnone, M.G.; Cusotto, S.; Fulling, C.; Golubeva, A.V.; et al. The microbiota-gut-brain axis. *Physiol. Rev.* **2019**, *99*, 1877–2013. [[CrossRef](#)]
11. Sasmita, A.O. Modification of the gut microbiome to combat neurodegeneration. *Rev. Neurosci.* **2019**, *30*, 795–805. [[CrossRef](#)]
12. Chen, S.G.; Stribinskis, V.; Rane, M.J.; Demuth, D.R.; Gozal, E.; Roberts, A.M.; Jagadapillai, R.; Liu, R.L.; Choe, K.W.; Shivakumar, B.; et al. Exposure to the functional bacterial amyloid protein curli enhances alpha-Synuclein aggregation in aged fischer 344 rats and *Caenorhabditis elegans*. *Sci. Rep.* **2016**, *6*, 34477. [[CrossRef](#)] [[PubMed](#)]
13. Friedland, R.P.; Chapman, M.R. The role of microbial amyloid in neurodegeneration. *PLoS Pathog.* **2017**, *13*, e1006654. [[CrossRef](#)] [[PubMed](#)]
14. Perov, S.; Lidor, O.; Salinas, N.; Golan, N.; Tayeb-Fligelman, E.; Deshmukh, M.; Willbold, D.; Landau, M. Structural insights into curli CsgA cross-beta fibril architecture inspire repurposing of anti-amyloid compounds as anti-biofilm agents. *PLoS Pathog.* **2019**, *15*, e1007978. [[CrossRef](#)]
15. Javed, I.; Zhang, Z.Z.; Adamcik, J.; Andrikopoulos, N.; Li, Y.H.; Otzen, D.E.; Lin, S.J.; Mezzenga, R.; Davis, T.P.; Ding, F.; et al. Accelerated amyloid beta pathogenesis by bacterial amyloid FapC. *Adv. Sci.* **2020**, *7*, 2001299. [[CrossRef](#)] [[PubMed](#)]
16. Schwartz, K.; Syed, A.K.; Stephenson, R.E.; Rickard, A.H.; Boles, B.R. Functional amyloids composed of phenol soluble modulins stabilize *Staphylococcus aureus* biofilms. *PLoS Pathog.* **2012**, *8*, e1002744. [[CrossRef](#)]
17. Cheung, G.Y.C.; Kretschmer, D.; Queck, S.Y.; Joo, H.S.; Wang, R.; Duong, A.C.; Nguyen, T.H.; Bach, T.H.L.; Porter, A.R.; DeLeo, F.R.; et al. Insight into structure-function relationship in phenol-soluble modulins using an alanine screen of the phenol-soluble modulins (PSM) $\alpha 3$ peptide. *Faseb. J.* **2014**, *28*, 153–161. [[CrossRef](#)]
18. Laabei, M.; Jamieson, W.D.; Yang, Y.; van den Eisen, J.; Jenkins, A.T.A. Investigating the lytic activity and structural properties of *Staphylococcus aureus* phenol soluble modulins (PSM) peptide toxins. *Biochim. Biophys. Acta-Biomembr.* **2014**, *1838*, 3153–3161. [[CrossRef](#)]
19. Tayeb-Fligelman, E.; Tabachnikov, O.; Moshe, A.; Goldshmidt-Tran, O.; Sawaya, M.R.; Coquelle, N.; Colletier, J.P.; Landau, M. The cytotoxic *Staphylococcus aureus* PSM $\alpha 3$ reveals a cross- α amyloid-like fibril. *Science* **2017**, *355*, 831–833. [[CrossRef](#)]
20. Zaman, M.; Andreasen, M. Cross-talk between individual phenol-soluble modulins in *Staphylococcus aureus* biofilm enables rapid and efficient amyloid formation. *Elife* **2020**, *9*, e59776. [[CrossRef](#)]
21. Festa, G.; Mallamace, F.; Sancesario, G.M.; Corsaro, C.; Mallamace, D.; Fazio, E.; Arcidiacono, L.; Garcia Sakai, V.; Senesi, R.; Preziosi, E. Aggregation states of A β _{1–40}, A β _{1–42} and A β _{P3–42} amyloid beta peptides: A SANS Study. *Int. J. Mol. Sci.* **2019**, *20*, 4126. [[CrossRef](#)] [[PubMed](#)]
22. Boopathi, S.; Kolandaivel, P. Role of zinc and copper metal ions in amyloid beta-peptides Abeta(1-40) and Abeta(1-42) aggregation. *RSC Adv.* **2014**, *4*, 38951–38965. [[CrossRef](#)]
23. Das, M.; Dash, S.; Bhargava, B.L. Computational studies of fibrillation induced selective cytotoxicity of cross-alpha amyloid—Phenol soluble modulins $\alpha 3$. *Chem. Phys.* **2020**, *535*, 110777. [[CrossRef](#)]
24. Trott, O.; Olson, A.J. Software news and update AutoDock Vina: Improving the speed and accuracy of docking with a new scoring function, efficient optimization, and multithreading. *Comput. Chem.* **2010**, *31*, 455–461.
25. Pronk, S.; Pall, S.; Schulz, R.; Larsson, P.; Bjelkmar, P.; Apostolov, R.; Shirts, M.R.; Smith, J.C.; Kasson, P.M.; van der Spoel, D.; et al. GROMACS 4.5: A high-throughput and highly parallel open source molecular simulation toolkit. *Bioinf.* **2013**, *29*, 845–854. [[CrossRef](#)]
26. Hornak, V.; Abel, R.; Okur, A.; Strockbine, B.; Roitberg, A.; Simmerling, C. Comparison of multiple amber force fields and development of improved protein backbone parameters. *Proteins Struct. Funct. Bioinf.* **2006**, *65*, 712–725. [[CrossRef](#)]
27. Steinczinger, Z.; Jovari, P.; Pusztai, L. Comparison of 9 classical interaction potentials of liquid water: Simultaneous reverse monte carlo modeling of X-ray and neutron diffraction results and partial radial distribution functions from computer simulations. *J. Mol. Liq.* **2017**, *228*, 19–24. [[CrossRef](#)]
28. Dzubiella, J. Salt-specific stability and denaturation of a short salt-bridge forming α -helix. *J. Am. Chem. Soc.* **2008**, *130*, 14000–14007. [[CrossRef](#)]
29. Triguero, L.; Singh, R.; Prabhakar, R. Comparative molecular dynamics studies of wild-type and oxidized forms of full-length Alzheimer amyloid- β peptides A β (1-40) and A β (1-42). *J. Phys. Chem. B* **2008**, *112*, 7123–7131. [[CrossRef](#)]
30. Kumari, R.; Kumar, R.; Lynn, A. g_mmpbsa—a GROMACS tool for high-throughput MM-PBSA calculations. *J. Chem. Inf. Model.* **2014**, *54*, 1951–1962. [[CrossRef](#)]
31. Jamasbi, E.; Hossain, M.A.; Tan, M.; Separovic, F.; Ciccotosto, G.D. Fluorescence imaging of the interaction of amyloid beta 40 peptides with live cells and model membrane. *Biochim. Biophys. Acta-Biomembr.* **2018**, *1860*, 1609–1615. [[CrossRef](#)] [[PubMed](#)]
32. Xue, C.; Lin, T.Y.W.; Chang, D.; Guo, Z.F. Thioflavin T as an amyloid dye: Fibril quantification, optimal concentration and effect on aggregation. *Soc. Open Sci.* **2017**, *4*, 160696. [[CrossRef](#)] [[PubMed](#)]
33. Le, K.Y.; Villaruz, A.E.; Zheng, Y.; He, L.; Fisher, E.L.; Nguyen, T.H.; Ho, T.V.; Yeh, A.J.; Joo, H.S.; Cheung, G.Y.C.; et al. Role of phenol-soluble modulins in *Staphylococcus epidermidis* biofilm formation and infection of indwelling medical devices. *J. Mol. Biol.* **2019**, *431*, 3015–3027. [[CrossRef](#)]
34. Tayeb-Fligelman, E.; Salinas, N.; Tabachnikov, O.; Landau, M. *Staphylococcus aureus* PSM $\alpha 3$ cross- α fibril polymorphism and determinants of cytotoxicity. *Structure* **2020**, *28*, 301–313. [[CrossRef](#)]

35. Bertini, I.; Gonnelli, L.; Luchinat, C.; Mao, J.F.; Nesi, A. A new structural model of Abeta(40) fibrils. *J. Am. Chem. Soc.* **2011**, *133*, 16013–16022. [[CrossRef](#)]
36. Meisl, G.; Kirkegaard, J.; Arosio, P.; Michaels, T.; Vendruscolo, M.; Dobson, C.; Linse, S.; Knowles, T. Molecular mechanisms of protein aggregation from global fitting of kinetic models. *Nat. Protoc.* **2016**, *11*, 252–272. [[CrossRef](#)]
37. Du, W.J.; Guo, J.J.; Gao, M.T.; Hu, S.Q.; Dong, X.Y.; Han, Y.F.; Liu, F.F.; Jiang, S.; Sun, Y. Brazilin inhibits amyloid β -protein fibrillogenesis, remodels amyloid fibrils and reduces amyloid cytotoxicity. *Sci. Rep.* **2015**, *5*, 7992. [[CrossRef](#)] [[PubMed](#)]
38. Pryor, N.E.; Moss, M.A.; Hestekin, C.N. Capillary electrophoresis for the analysis of the effect of sample preparation on early stages of Abeta(1-40) aggregation. *Electrophoresis* **2014**, *35*, 1814–1820. [[CrossRef](#)] [[PubMed](#)]
39. Adem, K.; Shanti, A.; Srivastava, A.; Homouz, D.; Thomas, S.; Khair, M.; Stefanini, C.; Chan, V.; Kim, T.; Lee, S. Linking Alzheimer's disease and type 2 diabetes: Characterization and inhibition of cytotoxic A β and IAPP hetero-aggregates. *Front. Mol. Biosci.* **2022**, *9*, 842582. [[CrossRef](#)]
40. Ge, X.W.; Yang, Y.; Sun, Y.X.; Cao, W.G.; Ding, F. Islet amyloid polypeptide promotes amyloid-beta aggregation by binding-induced helix-unfolding of the amyloidogenic core. *ACS Chem. Neurosci.* **2018**, *9*, 967–975. [[CrossRef](#)]
41. Ilitchev, A.I.; Giarnmona, M.J.; Schwarze, J.N.; Buratto, S.K.; Bowers, M.T. Zinc-induced conformational transitions in human islet amyloid polypeptide and their role in the inhibition of amyloidosis. *J. Phys. Chem. B* **2018**, *122*, 9852–9859. [[CrossRef](#)] [[PubMed](#)]
42. Ren, B.P.; Zhang, Y.X.; Zhang, M.Z.; Liu, Y.L.; Zhang, D.; Gong, X.; Feng, Z.Q.; Tang, J.X.; Chang, Y.; Zheng, J. Fundamentals of cross-seeding of amyloid proteins: An introduction. *J. Phys. Chem. B* **2019**, *7*, 7267–7282. [[CrossRef](#)] [[PubMed](#)]
43. Cohen, S.I.A.; Linse, S.; Luheshi, L.M.; Hellstrand, E.; White, D.A.; Rajah, L.; Otzen, D.E.; Vendruscolo, M.; Dobson, C.M.; Knowles, T.P.J. Proliferation of amyloid-beta 42 aggregates occurs through a secondary nucleation mechanism. *Proc. Natl. Acad. Sci. USA* **2013**, *110*, 9758–9763. [[CrossRef](#)] [[PubMed](#)]
44. Bharadwaj, P.; Solomon, T.; Sahoo, B.R. Amylin and beta amyloid proteins interact to form amorphous heterocomplexes with enhanced toxicity in neuronal cells. *Sci. Rep.* **2020**, *10*, 10356. [[CrossRef](#)]
45. Guo, J.P.; Arai, T.; Miklossy, J.; McGeer, P.L. Abeta and tau form soluble complexes that may promote self aggregation of both into the insoluble forms observed in Alzheimer's disease. *Proc. Natl. Acad. Sci. USA* **2006**, *103*, 1953–1958. [[CrossRef](#)]
46. Mandal, P.K.; Pettegrew, J.W.; Masliah, E.; Hamilton, R.L.; Mandal, R. Interaction between A beta peptide and alpha synuclein: Molecular mechanisms in overlapping pathology of Alzheimer's and Parkinson's in dementia with Lewy body disease. *Neurosci. Res.* **2006**, *31*, 1153–1162.
47. Sampson, T.R.; Challis, C.; Jain, N.; Moiseyenko, A.; Ladinsky, M.S.; Shastri, G.G.; Thron, T.; Needham, B.D.; Horvath, I.; Debelius, J.W.; et al. A gut bacterial amyloid promotes alpha-synuclein aggregation and motor impairment in mice. *Elife* **2020**, *9*, e53111. [[CrossRef](#)]
48. Li, X.H.; Lao, Z.H.; Zou, Y.; Dong, X.W.; Li, L.; Wei, G.H. Mechanistic Insights into the co-aggregation of A β and hIAPP: An all-atom molecular dynamic study. *J. Phys. Chem. B* **2021**, *125*, 2050–2060. [[CrossRef](#)]
49. Raz, Y.; Miller, Y. Interactions between A β and mutated tau lead to polymorphism and induce aggregation of A β -mutated tau oligomeric complexes. *PLoS ONE* **2013**, *8*, e73303. [[CrossRef](#)]
50. Bhattacharya, S.; Xu, L.; Thompson, D. Molecular simulations reveal terminal group mediated stabilization of helical conformers in both amyloid-beta 42 and α -Synuclein. *ACS Chem. Neurosci.* **2019**, *10*, 2830–2842. [[CrossRef](#)]
51. Hou, S.; Gu, R.X.; Wei, D.Q. Inhibition of beta-amyloid channels with a drug candidate wgx-50 revealed by molecular dynamics simulations. *J. Chem. Inf. Model.* **2017**, *57*, 2811–2821. [[CrossRef](#)] [[PubMed](#)]
52. Xu, S.Y.; Wang, W.J.; Dong, X.Y.; Sun, Y. Molecular insight into Cu²⁺-induced conformational transitions of amyloid beta-protein from fast kinetic analysis and molecular dynamics simulations. *ACS Chem. Neurosci.* **2021**, *12*, 300–310. [[CrossRef](#)] [[PubMed](#)]
53. Nie, R.Z.; Dang, M.Z.; Li, K.K.; Peng, J.M.; Du, J.; Zhang, M.Y.; Li, C.M. A-type EGCG dimer, a new proanthocyanidins dimer from persimmon fruits, interacts with the amino acid residues of Abeta(40) which possessed high aggregation-propensity and strongly inhibits its amyloid fibrils formation. *J. Funct. Foods* **2019**, *52*, 492–504. [[CrossRef](#)]
54. Carter, P.; Andersen, C.A.F.; Rost, B. DSSPcont: Continuous secondary structure assignments for proteins. *Nucleic Acids Res.* **2003**, *31*, 3293–3295. [[CrossRef](#)]
55. Saini, R.K.; Thakur, H.; Goyal, B. Effect of piedmont mutation (L34V) on the structure, dynamics, and aggregation of Alzheimer's abeta(40) peptide. *J. Mol. Graphics Modell.* **2020**, *97*, 107571. [[CrossRef](#)]
56. Linh, N.H.; Thu, T.T.M.; Tu, L.; Hu, C.K.; Li, M.S. Impact of mutations at C-terminus on structures and dynamics of Abeta 40 and Abeta 42: A molecular simulation study. *J. Phys. Chem. B* **2017**, *121*, 4341–4354. [[CrossRef](#)]
57. Kocis, P.; Tolar, M.; Yu, J.; Sinko, W.; Ray, S.; Blennow, K.; Fillit, H.; Hey, J.A. Elucidating the Abeta 42 anti-aggregation mechanism of action of tramiprosate in Alzheimer's Disease: Integrating molecular analytical methods, pharmacokinetic and clinical data. *CNS Drugs* **2017**, *31*, 495–509. [[CrossRef](#)]
58. Bartling, C.R.O.; Jensen, T.M.T.; Henry, S.M.; Colliander, A.L.; Sereikaite, V.; Wenzler, M.; Jain, P.; Maric, H.M.; Harpsoe, K.; Pedersen, S.W.; et al. Targeting the APP-Mint2 protein-protein interaction with a peptide-based inhibitor reduces amyloid-beta formation. *J. Am. Chem. Soc.* **2021**, *143*, 891–901. [[CrossRef](#)]
59. Urbanc, B. Flexible N-termini of amyloid beta-protein oligomers: A link between structure and activity? *Isr. J. Chem.* **2017**, *57*, 651–664. [[CrossRef](#)]
60. Miller, Y.; Ma, B.Y.; Nussinov, R. The unique Alzheimer's beta-amyloid triangular fibril has a cavity along the fibril axis under physiological conditions. *J. Am. Chem. Soc.* **2011**, *133*, 2742–2748. [[CrossRef](#)]

61. Andreetto, E.; Yan, L.M.; Caporale, A.; Kapurniotu, A. Dissecting the role of single regions of an IAPP mimic and IAPP in inhibition of Abeta 40 amyloid formation and cytotoxicity. *ChemBioChem*. **2011**, *12*, 1313–1322. [[CrossRef](#)] [[PubMed](#)]
62. Aftabizadeh, M.; Tatarek-Nossol, M.; Andreetto, E.; El Bounkari, O.; Kipp, M.; Beyer, C.; Kapurniotu, A. Blocking inflammasome activation caused by betaamyloid peptide (Abeta) and islet amyloid polypeptide (IAPP) through an IAPP mimic. *ACS Chem. Neurosci.* **2019**, *10*, 3703–3717. [[CrossRef](#)] [[PubMed](#)]
63. Belsare, K.D.; Wu, H.; Mondal, D.; Bond, A.; Castillo, E.; Jin, J.; Jo, H.; Roush, A.E.; Pilla, K.B.; Sali, A.; et al. Soluble TREM2 inhibits secondary nucleation of A β fibrillization and enhances cellular uptake of fibrillar A β . *Proc. Natl. Acad. Sci. USA* **2022**, *119*, e2114486119. [[CrossRef](#)] [[PubMed](#)]

Disclaimer/Publisher's Note: The statements, opinions and data contained in all publications are solely those of the individual author(s) and contributor(s) and not of MDPI and/or the editor(s). MDPI and/or the editor(s) disclaim responsibility for any injury to people or property resulting from any ideas, methods, instructions or products referred to in the content.